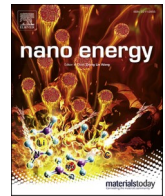




Contents lists available at ScienceDirect

Nano Energy

journal homepage: <http://www.elsevier.com/locate/nanoen>

Full paper

## Direct current triboelectric cell by sliding an n-type semiconductor on a p-type semiconductor

Ran Xu<sup>a</sup>, Qing Zhang<sup>a,\*</sup>, Jing Yuan Wang<sup>a</sup>, Di Liu<sup>b</sup>, Jie Wang<sup>b</sup>, Zhong Lin Wang<sup>b,c,\*\*</sup>

<sup>a</sup> School of Electrical & Electronic Engineering, Nanyang Technological University, 50 Nanyang Avenue, Singapore, 639798, Singapore

<sup>b</sup> Beijing Institute of Nanoenergy and Nanosystems, Chinese Academy of Sciences, Beijing, 100083, China

<sup>c</sup> School of Materials Science and Engineering, Georgia Institute of Technology, Atlanta, GA, 30332, USA

## ARTICLE INFO

## Keywords:

Direct current generators  
Triboelectric cells  
Doped semiconductors  
p-n junctions

## ABSTRACT

Triboelectric generators are a type of devices for harvesting mechanical energy by utilizing triboelectric and electrostatic induction effects. When two materials of different electron affinities are brought into contact, electrons transfer across the contacted surfaces owing to triboelectrification. When the two materials are slid against each other with a variation of the contacting surface area, an alternating current is electrostatically induced in the external circuit. In this paper, a novel electric generator, called triboelectric cell, based on sliding friction between n- and p-type doped semiconductors without changing the contacting area is reported. A direct current is generated in the direction of the built-in electric field in the dynamic p-n junction across the contacted surfaces, flowing from the p-semiconductor through the external circuit to the n-semiconductor. The generated currents and voltages are studied through sliding speeds, accelerations, contacting forces, operation temperatures and the geometries of the top electrode. The direct current generation can be attributed to electron-hole pairs generated at the two sliding surfaces, which are then swept out the dynamic junction by the built-in electric field.

### 1. Introduction

Mechanical-to-electric power conversion has been a hot research topic for several decades. Most electricity harvested from mechanical energy is in an alternating current (AC) form. However, in terms of the efficiency of utilizing in non-interrupted electronic, signal processing and electricity storage, direct current (DC) is more favorable. Electromagnetic generators convert mechanical power into electric power through Faraday's law of electromagnetic induction. The electricity generated is originally in AC form, but with a split ring commutator that switches the polarity of the conductor coil every half cycle, it is easy to obtain the current in DC. A big drawback for electromagnetic generators is its poor capability in miniaturization. Piezoelectric effect can be utilized to harvest mechanical energy. The Schottky contacts between piezoelectric ZnO nanomaterials [1–3] or conducting polymer Ppy [4] and metallic electrodes were reported to regulate electron motion more favorable toward one direction, resulting in a DC output. Another mechanical-to-electric power conversion technique that has been growing fast recently is through triboelectric process. In a typical

triboelectric nanogenerator (TENG), two materials with different electron affinities are brought together for contact triboelectrification, such that the material with a lower electron affinity gives away its electrons through the contacted surfaces to the other, resulting oppositely charged surfaces. With repeatedly changing the size of the contacting area by external mechanical force, the capacitance of the two electrodes varies, resulting electrons flow back and forth in the circuit to balance the varying potential difference, generating an AC current [5–11]. To convert an AC current in to a DC current, rectification approaches such as circuit configurations [12], generator electrode structure design such as wheel-belt [13] or electric brushes [14], etc. have to be engaged. In addition, several types of new generators could directly convert mechanical power into DC power. Using electrostatic breakdown between the two electrodes in a TENG, a DC current was created while the electrode is slid on the other [15], in which air gaps between collector electrode and triboelectrification layer as well as the air pressure play essential roles. In addition, sliding a metal tip on MoS<sub>2</sub> [16] or oxide layer on silicon [17] were reported to create DC currents. It was suggested that electrons generated at the contact surfaces by

\* Corresponding author.

\*\* Corresponding author. Beijing Institute of Nanoenergy and Nanosystems, Chinese Academy of Sciences, Beijing, 100083, China.

E-mail addresses: [qzhang@ntu.edu.sg](mailto:qzhang@ntu.edu.sg) (Q. Zhang), [zhong.wang@mse.gatech.edu](mailto:zhong.wang@mse.gatech.edu) (Z.L. Wang).

<https://doi.org/10.1016/j.nanoen.2019.104185>

Received 3 September 2019; Received in revised form 7 October 2019; Accepted 8 October 2019

Available online 12 October 2019

2211-2855/© 2019 Elsevier Ltd. All rights reserved.

triboelectrification tunnel through the ultrathin insulating layer, resulting in DC currents. Similarly, a DC current was found to be generated while a metal tip sliding on a Si substrate [18]. Although dynamic appearance and disappearance of the depletion layer in the Schottky junction was proposed to be the origin of the DC current generation, the detailed mechanism was not discussed. Previously, we have reported that by intermittently contacting and separating a p- and an n-type silicon electrode, a one-flow direction dominated AC current was achieved [19]. In this work, we report on DC current generation with a pair of p- and n-type doped semiconductors that are slid against each other without changing the size of the contacting area. The current flow direction is determined by the built-in electric field in the p-n junction across the two contacted surfaces, regardless of the relative sliding direction. Electron transport in the generator is analogous with

that in solar cells. The major difference is that electrons and holes in our generator are generated by triboelectrification, rather than photon excitation in solar cells. To differentiate from other electric generators, we call this new generator a triboelectric cell.

## 2. Experimental results and discussions

### 2.1. Direct current generation under sliding

When p- and n-type semiconductors are brought into contact, a p-n junction forms near the contacted surfaces with a built-in electric field pointing from the n-to the p-type surface. Here, we demonstrate that a DC current is generated as long as the two semiconductors are slid against each other. In all the experiments discussed in this paper, a pair

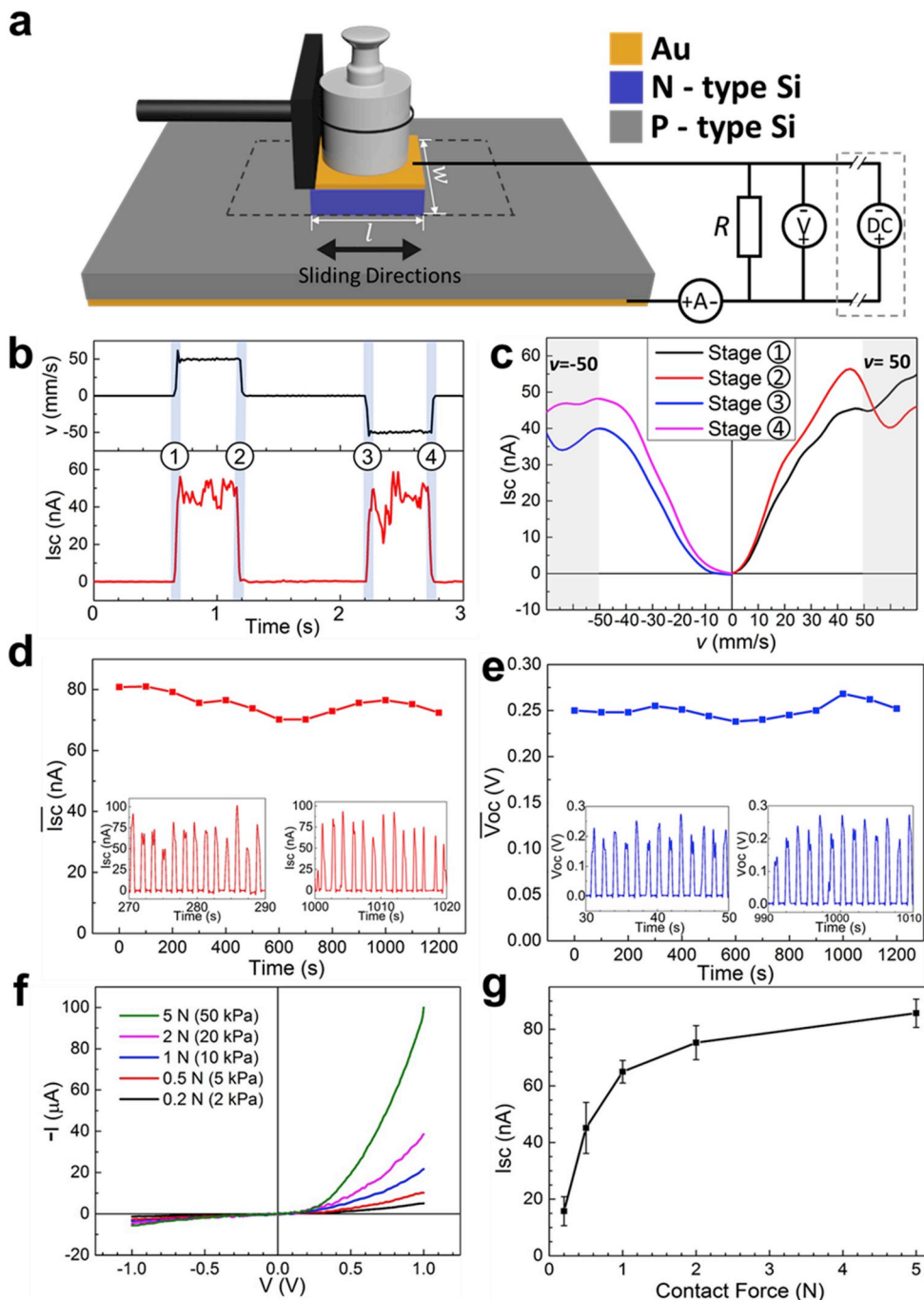


**Fig. 1.** Experimental set up and the typical output of the triboelectric cell. (a) A 3D schematics for the experiment setup and the external circuit. A  $1 \times 1$  cm<sup>2</sup> n-type silicon electrode was on a 4-inch p-type silicon wafer with 100 g weight on top (not to the scales). (b) The displacement (upper) of the top electrode with respect to the other electrode and  $I_{sc}$  (lower) as a function of time for four sliding stages in one sliding cycle. (c)  $I_{sc}$  as a function of the sliding speed for the four sliding stages in (b). (d)  $I_{sc}$  and (e)  $V_{oc}$  for 20 min sliding experiments. (f) The I-V curves of the two contacted electrodes under a normal force from 0.2 N to 5 N and (g)  $I_{sc}$  measured when sliding at 50 mm s<sup>-1</sup> under various normal forces.

of n- and p-doped semiconductor substrates or a pair of doped semiconductor and a metal is utilized directly as the electrodes. One of the substrates is cut into a smaller size and placed onto the other so that the two flat surfaces face each other. The small electrode can be slid or rotated on the large one, as shown in Fig. 1a. For instance, a  $1 \times 1 \text{ cm}^2$  n-doped silicon electrode was slid on a p-doped silicon electrode back and forth repeatedly on a linear motor controlled translation stage. On top of the moving electrode, a 100 g weight was engaged to achieve 1 N normal force. Fig. 1b shows an arbitrary cycle for sliding at a constant speed of  $50 \text{ mm s}^{-1}$ . A continuous DC current about 50 nA was generated during the movement regardless of the sliding direction. In Stage 1 (3), the top electrode was slid forward (backward) from the rest to the constant speed at an acceleration of  $5 \text{ m s}^{-2}$ . In contrast, in Stages 2 and 4, the top electrode was decelerated at  $5 \text{ m s}^{-2}$  to a full stop. The short circuit current,  $I_{\text{SC}}$ , with respect to instantaneous speed for each stage clearly indicated that the current could respond to the transient speed immediately, no hysteresis loop was observed in the experimental error, see Fig. 1c. The DC current always flew from the p-silicon through the external circuit to the n-silicon electrode. Once the sliding was stopped, the current dropped to zero instantaneously. With continuous sliding, a constant DC can be observed. Fig. S1 shows a DC short circuit current when the n-type electrode was slid 30 mm away from the centre of a rotating p-type electrode with a constant angular speed of 10 rpm controlled by a rotation stage. The current fluctuation could be associated with the stick-slip behavior, caused by microscopic friction fluctuation, possibly resulted from friction force variation in different sliding regimes [20,21]. Fig. 1d and e plot the average  $I_{\text{SC}}$  and open circuit voltage,  $V_{\text{OC}}$ , over 20 min with a 2-s pause after each sliding to either direction, respectively. No obvious decay of the output was observed over time.

Formation of the p-n junction across the contacted surfaces can be confirmed by clear rectification characteristics, as shown in Fig. 1f. Under a force of 0.2 N (or an apparent pressure of 2 kPa), the overall current was small and the rectification factor,  $|I_{\text{F}}(1\text{V})/I_{\text{R}}(-1\text{V})|$ , was only 4.5. With increasing the contact force (pressure) up to 5 N (50 kPa), the rectification performance was improved with the rectification factor increasing up to 20.  $I_{\text{SC}}$  increased from 16.5 nA under a force of 0.2 N to 89 nA under 5 N, see Fig. 1g.  $I_{\text{SC}}$  turned to saturation when the force was larger than 2 N. The force could affect the generated current in two possible ways. A larger contact force (or apparent pressure) leads to a diminution of air gaps between the two contact surfaces and increases effective contact area and hence improve the electrical contact. Furthermore, increasing the force (or pressure) results in larger frictional force or higher frictional power that excites more electrons and holes.

A 1  $\mu\text{F}$  capacitor was employed to collect the charge from the DC current. The voltage over the capacitor could saturate at 0.28 V with 4 back-and-forth sliding cycles (see Fig. S2). The saturated voltage is constrained by the built-in potential of the contacted p-n junction, which should correspond to the chemical potential difference (opposite to the work function difference) between the two electrodes used here, i.e., 0.35 V measured using a variable capacitance technique (Refer to the Supporting Information and Fig. S4c).

Besides sliding a silicon electrode on another silicon electrode, we have confirmed in general that sliding a doped semiconductor electrode on another doped semiconductors or metals generates a DC current as long as the two electrode materials have distinct chemical potentials (or work functions). The generated currents from the electrode pairs of oppositely doped GaAs & silicon, p-type silicon & Al and n-type silicon & Au are displayed in Figs. S5–S10 in the Supporting Information. The common feature of all the tested electrode pairs is that the generated DC current flows from the lower chemical potential (or higher work functions) electrode through the external circuit to the other electrode, which is in the direction consistent with the direction of the built-in electric field in the p-n junction across the contacted surfaces, suggesting that electrons and holes are generated by frictional energy and then

swept out of the p-n junction to form the DC current. In our approach, the size of the contacted area during the sliding was unchanged. This is different from the sliding mode of typical TENGs [9–11] where the current is created by electrostatic induction due to variation of the contacted surface area.

## 2.2. Influences of the sliding speed and acceleration

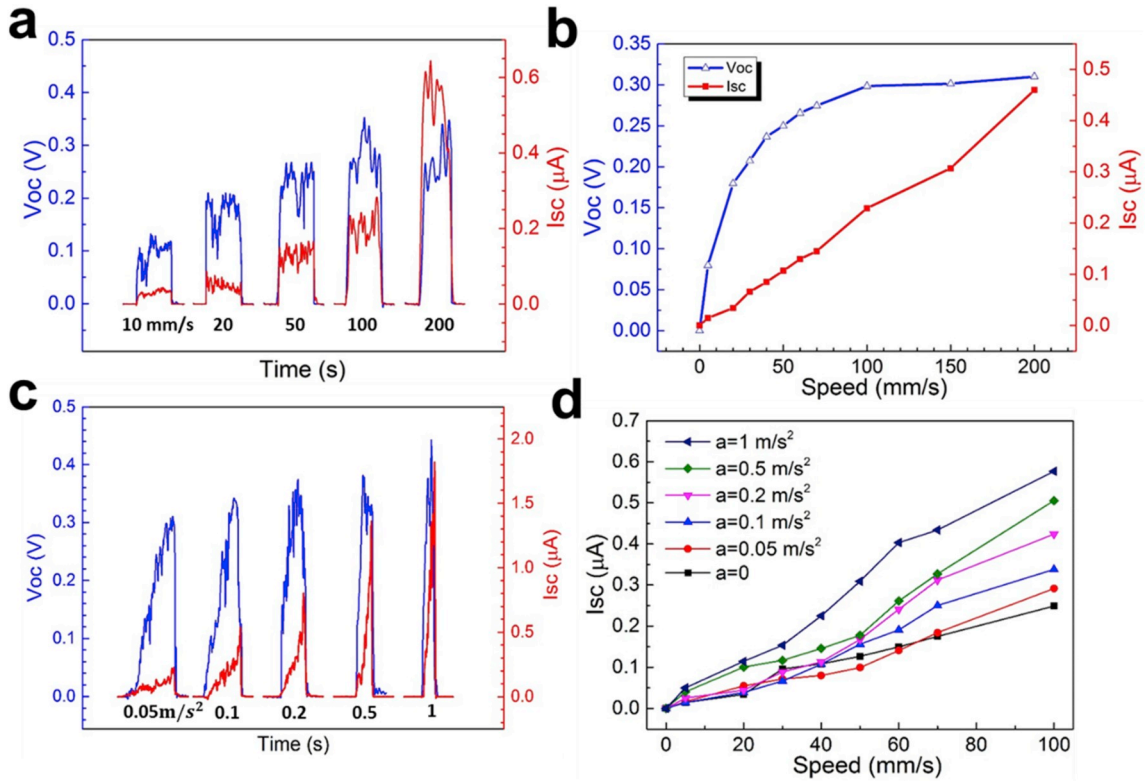
Macroscopically, the sliding speed  $v$  is directly related to the friction power as  $P_f = \mu_s Fv$ , where  $F$  is the normal force and  $\mu_s$  refers to the sliding friction coefficient that is independent of the apparent contact area and sliding velocity [22]. With the experimental conditions in this work,  $\mu_s$  is estimated to be 0.2 [23,24]. This friction power dissipates in the contact surfaces, causing excitation of electrons and holes. Thus, the number of generated electron-hole pairs is expected to be linearly proportional to the friction power or the sliding speed.

Fig. 2a and b shows  $I_{\text{SC}}$  and  $V_{\text{OC}}$  under several constant sliding speeds with a weight of 100 g on top of a p-type electrode sliding on an n-type substrate.  $I_{\text{SC}}$  increased linearly by 10 times with the constant speed increasing from  $10 \text{ mm s}^{-1}$  to  $200 \text{ mm s}^{-1}$ , as shown in Fig. 2b. A higher sliding speed contributes a higher friction power, exciting more electrons and holes at the contact surfaces, which are subsequently swept out of the p-n junction by the built-in electric field, leading to a larger DC current. It is worth noting that, for the speed higher than  $100 \text{ mm s}^{-1}$ ,  $V_{\text{OC}}$  saturated at 0.31 V, which corresponded to the chemical potential difference of 0.35 V between the two electrodes, see Fig. S4c. Observed  $V_{\text{OC}}$  can be understood as the result of charging the parasitic capacitance in the device and circuit. The higher the speed, the more electrons and holes were generated and the quicker was the parasitic capacitor charged. The power dissipated to the load under a constant sliding of  $50 \text{ mm s}^{-1}$  is shown in Fig. S3. It maximized around  $1 \text{ M}\Omega$  at 1.2 nW. Note that the friction power can be estimated as  $P_f = \mu Fv \sim 10 \text{ mW}$ . Thus, the efficiency of the power conversion was  $\sim 1.2 \text{ nW}/10 \text{ mW} \sim 10^{-7}$ .

The influences of transient sliding speeds on  $V_{\text{OC}}$  and  $I_{\text{SC}}$  were studied using several accelerations from  $0.05 \text{ m s}^{-2}$  to  $1 \text{ m s}^{-2}$  (Fig. 2c). It is seen from Fig. 2d that  $I_{\text{SC}}$  at  $100 \text{ mm s}^{-1}$  increased from about  $0.23 \mu\text{A}$  for an acceleration of  $0 \text{ m s}^{-2}$  (the constant speeds as discussed above) to  $0.58 \mu\text{A}$  under  $1 \text{ m s}^{-2}$ . This suggests that the acceleration process could more efficiently excite electrons and holes than the constant speed process. The increase in friction power  $\Delta P_f$  from  $t = t_0$  to  $t = t_0 + \delta t$  is zero for a constant speed motion, while it is equal to  $\mu_s F a \delta t$  for an accelerated motion with an acceleration  $a$  (see Supporting Information). Thus, the additional power gain increases with acceleration and it is dissipated to the contacted surfaces and hence enhances the excitation of electrons and holes. Moreover, the mechanical power dissipated to the surfaces under a smaller acceleration may form a temperature profile through which heat could transport into the bulk of the doped semiconductor electrodes, leading to weaker electron-hole generation near the surfaces.

## 2.3. Influences of the geometry of the top electrode

With the same apparent contact area (or the area of the top electrode), normal force, sliding speed and sliding distance, the influence of the geometry of the top electrode was studied by using three different lengths of the sliding sides (perpendicular to the sliding direction,  $w$  in Fig. 1a). It can be seen from Fig. 3 that the larger the side length, the higher  $I_{\text{SC}}$  could be obtained. In contrast,  $V_{\text{OC}}$  did not vary significantly. These findings suggest the length of the sliding side dominated  $I_{\text{SC}}$ , rather than the apparent contact area of the two electrodes. This is because that when the top electrode is slid under the same contact pressure (through controlling the contact area and normal force) and sliding speed, the newly established p-n junction in front and the disappeared former p-n junction at the back are larger for the samples with a larger  $w$ . Hence, a larger temporal change in surface dipoles could be caused (refer to more detailed discussion in Section 3), generating more



**Fig. 2.**  $I_{SC}$  and  $V_{OC}$  against the transient speeds and accelerations. (a)  $I_{SC}$  and  $V_{OC}$  vs time under different constant sliding speeds from  $10 \text{ mm s}^{-1}$  to  $200 \text{ mm s}^{-1}$ ; (b)  $I_{SC}$  and  $V_{OC}$  vs the sliding speed; (c)  $I_{SC}$  and  $V_{OC}$  vs time under different accelerations from  $0.05 \text{ m s}^{-2}$  to  $1 \text{ m s}^{-2}$ ; (d)  $I_{SC}$  vs the transient speed under different accelerations.

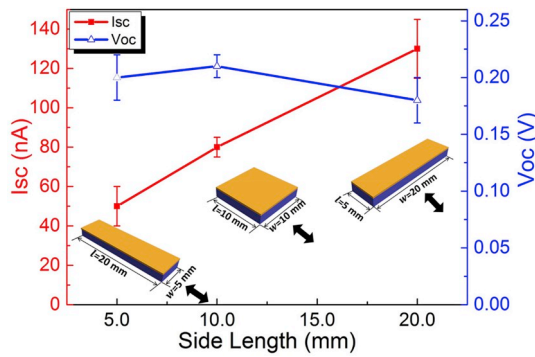


**Fig. 3.**  $I_{SC}$  and  $V_{OC}$  against the length of the sliding side of three top electrodes with same apparent contact area but increasing side lengths.

electrons and holes. In other words, only the new overlapping/releasing regions efficiently promote charge transfer. This characteristic of our devices is similar to the sliding mode of triboelectric nanogenerators.

#### 2.4. Influences of operational pressure, humidity and temperature

To investigate the influences of air pressure on the DC current generation, the sliding experiments were performed in a vacuum chamber under the air pressure of  $10^{-5} \text{ Pa}$ , and after that, the vacuum chamber was refilled with nitrogen up to the atmosphere.  $I_{SC}$  generated in the vacuum was found to be comparable with those measured under nitrogen at atmosphere and air at atmosphere, as shown in Fig. 4a. This means that nitrogen, air and moisture should not be necessary factors contributed to the DC current generation.

Fig. 4b shows under  $10^{-5} \text{ Pa}$ , and the average  $I_{SC}$  was decreased from 150 nA at the room temperature down to only 50 nA at  $120^\circ \text{C}$ . This

phenomenon may be interpreted through the temperature dependent built-in potential. When the temperature increases, the Fermi levels in both semiconductor electrodes shift towards to the bandgap centre, leading to decrease in the built-in potential or built-in electric field and, consequently, decrease in the current generated.

### 3. Current generation in the triboelectric cell

In this discussion, the surfaces of the semiconductor electrodes are assumed ideal, and the influences of the surface states on the energy band diagram and electron transport are ignored. Fig. 5a shows the energy band diagrams for the two disconnected electrodes. The electrostatic potential of the p-type neutral region with respect to the Fermi level  $E_F$  is determined by  $\psi_1 \equiv -1/q(E_i - E_F) = -kT/q \ln(N_A/n_i)$ , where  $q$  is the unit charge,  $N_A$  is the acceptor concentration,  $E_i$  is the intrinsic Fermi level,  $k$  is the Boltzmann constant,  $T$  is the absolute temperature in Kelvin degree and  $n_i$  is the intrinsic carrier concentration. Correspondingly, the electrostatic potential of the n-type neutral region with respect to  $E_F$  is  $\psi_2 = kT/q \ln(N_D/n_i)$ , where  $N_D$  is the donor concentration [25]. When the electrodes are in contact (Fig. 5b), electrons diffuse from the n-type (E2) to the p-type semiconductor electrode (E1) (and holes diffuse from E1 to E2) due to their chemical potential difference, leading to formation of a p-n junction across the two contacted surfaces. As a result, positively charged space charges are left in the depletion region in the n-type semiconductor, while the negatively charged ones dwell in the p-type side, causing a built-in electric field pointing from n-to p-type semiconductor electrode in the junction. At the thermal equilibrium, a common flat Fermi level establishes across the two entire electrodes, leading to a built-in potential in the p-n junction [25].

$$V_{bi} = \psi_2 - \psi_1 = kT/q \ln(N_A N_D / n_i^2) \quad (1)$$



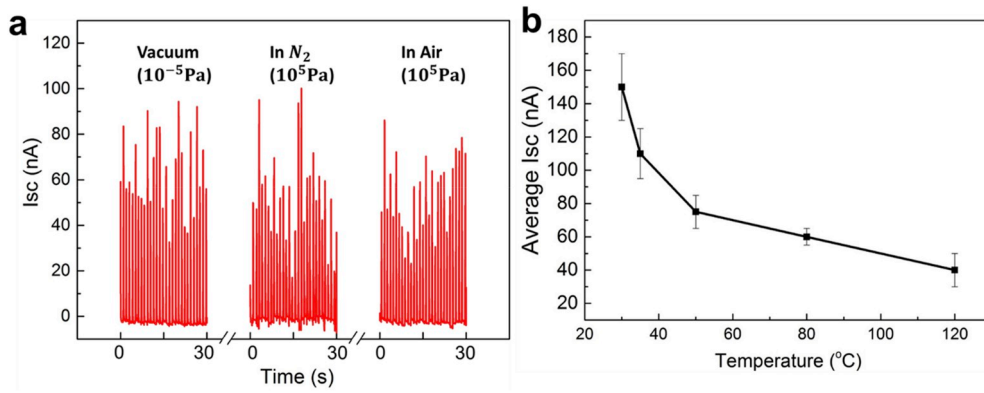


**Fig. 4.**  $I_{sc}$  measured in different environments and temperatures. (a)  $I_{sc}$  measured in vacuum ( $10^{-5}$  Pa) and in nitrogen/air atmosphere ( $10^5$  Pa). (b)  $I_{sc}$  measured in vacuum ( $10^{-5}$  Pa) with temperature increasing from room temperature to 120 °C.

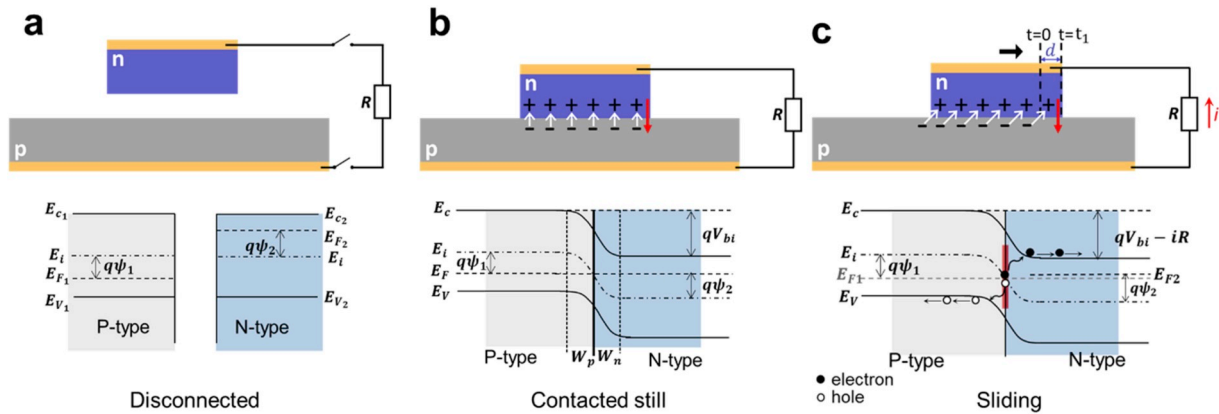


**Fig. 5.** The schematics and energy band diagrams for a triboelectric cell with an n-type semiconductor as the top electrode and a p-type semiconductor as the bottom electrode. (a) The disconnected stage, (b) the contacted still stage, (c) the top is being slid on the bottom electrode laterally. The white arrows stand for surface electric dipole moment; red arrow stands for built-in field direction.  $E_c$  is the bottom of the conduction band,  $E_v$  the top of the valence band,  $E_i$  the intrinsic level and  $E_F$  the Fermi level,  $V_{bi}$  the built-in potential,  $\psi_{1,2}$  are the potentials with respect to the Fermi levels in the p- and n-type semiconductors.

and zero current flowing in the external circuit.

DC current generation was obtained from sliding a metal electrode on a semiconductor [18] and it was attributed to acceleration or recoiling of electrons and holes that are diffusing across the depletion layer during the dynamic appearance and disappearance of the contacted Schottky junction. This interpretation seems not persuasive by the fact that the formation of the depletion layer is caused by diffusing charge carriers at the interface first and then the diffusion is confined by the space charge induced built-in electric field.

Herein, we interpret the DC current generation in triboelectric cells through the following possible processes:

- (1) Electrons and holes are generated due to the energy released by breaking of the bonds across the contacted surfaces in the friction sliding motion [26,27], and they can be expelled out of the p-n junction due to the built-in electric field, forming a DC current.
- (2) Because of overall charge neutrality, the space charges in the p-n junction can be regarded as an effective dipole whose dipole moment points from the negatively charged space charges in the p-type electrode to the positively charged space charges in the n-type electrode, perpendicular to the contacted surfaces under the thermal equilibrium. When the top electrode is being slid, the space charge region in the bottom electrode would follow the sliding motion, but with a small lagged distance of  $d \sim \nu\tau$  (see Fig. 5c), where  $\tau$  is the dielectric relaxation time and  $\nu$  is the sliding speed. As a result, the effective dipole moment slightly deviates from that under the thermal equilibrium, causing a

change in the potential energy of the dipole. This released energy from the newly formed dipole could excite electrons and holes in the lagged region with an area of  $w d \sim w\nu\tau$ . This could interpret our main findings discussed above, i.e.,  $I_{sc}$  is a linear function of  $\nu$  and  $I_{sc}$  is linearly proportional to  $w$ , rather than the area of the top electrode.

- (3) A surface flexoelectric potential difference could be induced by inhomogeneous strains at nanoscale asperities and it could promote electrons transferring from one surface to the other in contact [28]. In our case, sliding a semiconductor on another would definitely cause inhomogeneous strains between the two surface asperities.
- (4) As mentioned in the introduction, utilizing electrostatic breakdown of the small gap between the two electrodes of a TENG, photons could be created at the gap due to air discharge. Thus, a DC current was created while one electrode is slid on the other due to photon excitation [15]. However, this picture may not be applicable to our triboelectric cells. Firstly, for electrodes used in this paper, with one lightly doped n-type silicon electrode in contact with one highly doped p-type silicon electrode, the electric field at the interface between the two electrodes for an ideal p-n junction can be calculated as  $E_{max} = -(2q/\epsilon N_A V_{bi})^{1/2} \sim 3 \times 10^6 \text{ V m}^{-1}$ , where  $\epsilon$  is the permittivity of silicon. The electric field is much smaller than the air breakdown field of  $1 \times 10^8 \text{ V m}^{-1}$  required in small gaps [29,30]. Considering very large surface states and non-ideal p-n junction, the actual electric

field across the two contacted surfaces over the gap could be even lower. Secondly, air breakdown discharge would occur once the electrodes are contacted. It would not be promoted by the sliding. However, as shown in Fig. 1b, no current was generated if the top electrode was not slid. Thirdly, the DC current generation was not detectably affected when the electrodes were slid in vacuum or atmosphere.

It is worth pointing out that current generation in a triboelectric cell is essentially different from that in a typical sliding mode TENG in several aspects: (i) instead of utilizing an insulator surface of the electrode to retain electrostatic charges on the surface in the TENG, oppositely doped semiconductors are directly employed as electrodes in the triboelectric cell to form a p-n junction. (ii) The ratio of the contacted and un-contacted areas between two electrodes must be varied in a conventional sliding TENGs, while the size of the contacting area maintains unchanged during sliding for the triboelectric cell. It is the built-in electric field that drives the triboelectrically generated electrons and holes to form a DC current, rather than electrostatic induction between the electrodes in TENGs. (iii) There is only displacement current, no conduction current, directly across the two electrodes in conventional sliding TENGs, while in the triboelectric cell only conduction current is generated.

Electron transport in a triboelectric cell resembles in a semiconductor solar cell. The p-n junctions play a role in separating electrons and holes. In solar cells, electrons and holes are generated through absorbing photons [31]. In contrast, the electrons and holes in triboelectric cells are created by triboelectrification.

#### 4. Conclusion

In this work, direct current generation has been clearly demonstrated by sliding a doped semiconductor electrode against another oppositely doped semiconductor or metal electrode as long as the two electrodes are of distinct Fermi levels. The generated DC current flows in the same direction as that of the built-in electric field in the dynamic p-n (or Schottky) junction near the contacted surfaces and it does not depend on the sliding direction. It increases with the sliding speed and acceleration, decreases with increasing operational temperature and does not depend on atmospheric pressure. At a given speed, transient sliding could more efficiently generate the current than constant sliding. Our findings suggest that electrons and holes are generated at the contacted surfaces and then swept out of the contacted p-n (or Schottky) junction by the built-in electric field to form the DC current.

#### Declaration of competing interest

The authors declare that they have no known competing financial interests or personal relationships that could have appeared to influence the work reported in this paper.

#### Acknowledgements

This project is financially supported by the ignition fund of School of EEE, Nanyang Technological University, Singapore, and MOE AcRF Tier1 (2018-T1-005-001), MOE AcRF Tier2 (2018-T2-2-005) and A\*STAR AME IRG Grant SERC A1983c0027, Singapore, the National Key R & D Project from Minister of Science and Technology, China (2016YFA0202704) and Chinese Academy of Sciences.

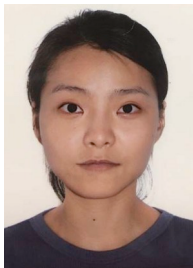
#### Appendix A. Supplementary data

Supplementary data to this article can be found online at <https://doi.org/10.1016/j.nanoen.2019.104185>.

#### References

- [1] X. Wang, J. Song, J. Lin, Z.L. Wang, Direct-current nanogenerator driven by ultrasonic waves, *Science* 316 (2007) 102–105, <https://doi.org/10.1126/science.1139366>.
- [2] G.C. Yoon, K.S. Shin, M.K. Gupta, K.Y. Lee, J.H. Lee, Z.L. Wang, S.W. Kim, High-performance hybrid cell based on an organic photovoltaic device and a direct current piezoelectric nanogenerator, *Nano Energy* 12 (2015) 547–555, <https://doi.org/10.1016/j.nanoen.2015.01.028>.
- [3] M.Y. Choi, D.H. Choi, M.J. Jin, I.S. Kim, S.H. Kim, J.Y. Choi, S.Y. Lee, J.M. Kim, S.W. Kim, Mechanically powered transparent flexible charge-generating nanodevices with piezoelectric ZnO nanorods, *Adv. Mater.* 21 (2009) 2185–2189, <https://doi.org/10.1002/adma.200803605>.
- [4] H. Shao, J. Fang, H. Wang, L. Dai, L. Tong, Polymer-metal Schottky contact with direct - current outputs, *Adv. Mater.* 28 (2016) 1461–1466, <https://doi.org/10.1002/adma.201504778>.
- [5] G. Zhu, B. Peng, J. Chen, Q. Jing, Z.L. Wang, Triboelectric nanogenerators as a new energy technology: from fundamentals, devices, to applications, *Nano Energy* 14 (2015) 126–138, <https://doi.org/10.1016/j.nanoen.2014.11.050>.
- [6] Q. Jing, G. Zhu, P. Bai, Y. Xie, J. Chen, R.P.S. Han, Z.L. Wang, Case-encapsulated triboelectric nanogenerator for harvesting energy from reciprocating sliding motion, *ACS Nano* 8 (2014) 3836–3842, <https://doi.org/10.1021/nm500694y>.
- [7] G. Zhu, J. Chen, T. Zhang, Q. Jing, Z.L. Wang, Radial-arrayed rotary electrification for high performance triboelectric generator, *Nat. Commun.* 5 (2014) 3426, <https://doi.org/10.1038/ncomms4426>.
- [8] G. Zhu, et al., A shape-adaptive thin-film-based approach for 50% high-efficiency energy generation through micro-grating sliding electrification, *Adv. Mater.* 26 (2014) 3788–3796, <https://doi.org/10.1002/adma.201400021>.
- [9] S. Niu, Y. Liu, S. Wang, L. Lin, Y. Zhou, Y. Hu, Z.L. Wang, Theoretical of sliding-mode triboelectric nanogenerators, *Adv. Mater.* 25 (2013) 6184–6193, <https://doi.org/10.1002/adma.201302808>.
- [10] S. Niu, S. Wang, L. Lin, Y. Zhou, Y. Hu, Z.L. Wang, Theoretical study of contact-mode triboelectric nanogenerators as an effective power source, *Energy Environ. Sci.* 6 (2013) 3576–3583, <https://doi.org/10.1039/C3EE42571A>.
- [11] C. Zhang, W. Tang, C. Ham, F. Fan, Z.L. Wang, Theoretical comparison, equivalent transformation, and conjunction operations of electromagnetic induction generator and triboelectric nanogenerator for harvesting mechanical energy, *Adv. Mater.* 26 (2014) 3580–3591, <https://doi.org/10.1002/adma.201400207>.
- [12] W.S. Jung, M.G. Kang, H.G. Moon, S.H. Baek, S.J. Yoon, Z.L. Wang, S.W. Kim, C. Y. Kang, High output piezo/triboelectric hybrid generator, *Sci. Rep.* 5 (2015) 9309, <https://doi.org/10.1038/srep09309>.
- [13] Y. Yang, H. Zhang, Z.L. Wang, Direct-current triboelectric generator, *Adv. Funct. Mater.* 24 (2014) 3745–3750, <https://doi.org/10.1002/adfm.201304295>.
- [14] C. Zhang, T. Zhou, W. Tang, C. Han, L. Zhang, Z.L. Wang, Rotating-disk-based direct-current triboelectric nanogenerator, *Adv. Energy Mater.* 4 (2014), <https://doi.org/10.1002/aenm.201301798>.
- [15] D. Liu, X. Yin, H. Guo, L. Zhou, X. Li, C. Zhang, J. Wang, Z.L. Wang, A constant current triboelectric nanogenerator arising from electrostatic breakdown, *Sci. Adv.* 5 (2019) 6437, <https://doi.org/10.1126/sciadv.aav6437>.
- [16] J. Liu, A. Goswami, K. Jiang, F. Khan, S. Kim, R. McGee, Z. Li, Z. Hu, J. Lee, T. Thundat, Direct-current triboelectricity generation by a sliding Schottky nanocontact on MoS<sub>2</sub> multilayers, *Nat. Nanotechnol.* 13 (2018) 112, <https://doi.org/10.1038/s41565-017-0019-5>.
- [17] J. Liu, M. Miao, K. Jiang, F. Khan, A. Goswami, R. McGee, Z. Li, L. Nguyen, Z. Hu, J. Lee, Sustained electron tunneling at unbiased metal-insulator-semiconductor triboelectric contacts, *Nano Energy* 48 (2018) 320–326, <https://doi.org/10.1016/j.nanoen.2018.03.068>.
- [18] S. Lin, Y. Lu, S. Feng, Z. Hao, Y. Yan, A high current density direct-current generator based on a moving van der Waals Schottky diode, *Adv. Mater.* 31 (2019), e1804398, <https://doi.org/10.1002/adma.201804398>.
- [19] Q. Zhang, R. Xu, W. Cai, Pumping electrons from chemical potential difference, *Nano Energy* 51 (2018) 698–703, <https://doi.org/10.1016/j.nanoen.2018.07.016>.
- [20] V. Lampaert, J. Swevers, F. Al-Bender, Modification of the Leuven integrated friction model structure, *IEEE Trans. Autom. Control* 47 (2002) 683–687, <https://doi.org/10.1109/9.995050>.
- [21] F. Al-Bender, V. Lampaert, J. Swevers, The generalized Maxwell-slip model: a novel model for friction simulation and compensation, *IEEE Trans. Autom. Control* 50 (2005) 1883–1887, <https://doi.org/10.1109/TAC.2005.858676>.
- [22] I. Hutchings, P. Shipway, *Tribology: Friction and Wear of Engineering Materials, second ed.*, Butterworth-Heinemann, 2017.
- [23] J.E. Dunkin, D.E. Kim, Measurement of static friction coefficient between flat surfaces, *Wear* 193 (1996) 186–192, [https://doi.org/10.1016/0043-1648\(95\)06706-X](https://doi.org/10.1016/0043-1648(95)06706-X).
- [24] D.C. Cranmer, Friction and wear properties of monolithic silicon-based ceramics, *J. Mater. Sci.* 20 (1985) 2029–2037, <https://doi.org/10.1007/BF01112286>.
- [25] S.M. Sze, K.K. Ng, *Physics of Semiconductor Devices, third ed.*, John Wiley & sons, New Jersey, 2006.
- [26] C. Xu, A. Wang, H. Zou, B. Zhang, C. Zhang, Y. Zi, L. Pan, P. Wang, P. Feng, Z. Lin, Raising the working temperature of a triboelectric nanogenerator by quenching down electron thermionic emission in contact-electrification, *Adv. Mater.* 30 (2018) 1803968, <https://doi.org/10.1002/adma.201803968>.
- [27] C. Xu, Y. Zi, A. Wang, H. Zou, Y. Dai, X. He, P. Wang, Y. Wang, P. Feng, D. Li, On the electron-transfer mechanism in the contact-electrification effect, *Adv. Mater.* 30 (2018) 1706790, <https://doi.org/10.1002/adma.201706790>.

- [28] C.A. Mizzi, A.Y.W. Lin, L.D. Marks, Does flexoelectricity drive triboelectricity? *Phys. Rev. Lett.* 123 (2019) 116103, <https://doi.org/10.1103/PhysRevLett.123.116103>.
- [29] E. Hourdakis, B.J. Simonds, N.M. Zimmerman, Submicron gap capacitor for measurement of breakdown voltage in air, *Rev. Sci. Instrum.* 77 (2006), 034702, <https://doi.org/10.1063/1.2185149>.
- [30] T. Ono, D.Y. Sim, M. Esashi, Micro-discharge and electric breakdown in a micro-gap, *J. Micromech. Microeng.* 10 (2000) 445.
- [31] J. Nelson, *The Physics of Solar Cells*, Imperial College Press, London, 2003.



**Ran Xu** is currently a Ph.D. candidate in School of Electrical and Electronic Engineering, Nanyang Technological University (NTU), Singapore. She received his B.S degree from School of Electrical and Electronic Engineering, Nanyang Technological University in 2015. Her research interests are in the area of generators based on semiconductor and triboelectric materials.



**Di Liu** received his B. S. degree in Material Science and Engineering from Nanjing University of Aeronautics and Astronautics. Now he is a Ph.D. candidate in Beijing Institute of Nanoenergy and Nanosystems, Chinese Academy of Sciences, China. His current research interest is triboelectric nanogenerators for energy harvesting and self-powered systems.



**Dr. Jie Wang** received her Ph.D. degree from Xi'an Jiaotong University in 2008. He is currently a professor at Beijing Institute of Nanoenergy and Nanosystems, Chinese Academy of Sciences. His current research interests focus on the energy materials, supercapacitors, nanogenerators and self-powered system.



**Prof. Qing Zhang** is the Director of Centre of Micro-/Nano-electronics in School of Electrical and Electronic Engineering, Nanyang Technological University (NTU), Singapore. His research interests cover nanomaterials and nano/micro-electronic devices, carbon/silicon based thin films, etc. His attention focuses on carbon nanotube and nanostructure-based devices and fundamentals, etc. He and his group members have studied functionalized carbon nanotubes for several types of sensors, logic circuits and Li-ion batteries, etc. He has published more than 250 peer-review scientific papers in the fields of electronic materials, physics and devices for data processing, sensing and energy storage and harvesting.



**Prof. Zhong Lin (ZL) Wang** is the Hightower Chair in Materials Science and Engineering and Regents' Professor at Georgia Tech, the chief scientist and director of the Beijing Institute of Nanoenergy and Nanosystems, Chinese Academy of Sciences. His discovery and breakthroughs in developing nanogenerators and self-powered nanosystems establish the principle and technological road map for harvesting mechanical energy from environmental and biological systems for powering personal electronics and future sensor networks. He coined and pioneered the field of piezotronics and piezophototronics.



**Jingyuan Wang** is a PhD candidate under the supervision of Prof Qing Zhang in NOVITAS, Nanoelectronics Centre of Excellence, School of Electrical and Electronic Engineering, Nanyang Technological University, Singapore. He received his B.Eng from School of Materials Science and Engineering at Nanyang Technological University in 2012. His research interest focuses on the design, preparation and application of supercapacitor materials for energy storage.